

RESEARCH ARTICLE

[View Article Online](#)  
[View Journal](#) | [View Issue](#)



Cite this: *Inorg. Chem. Front.*, 2025,  
12, 701

## Exploration of functional group effects on D<sub>2</sub>/H<sub>2</sub> separation selectivity within the UiO-66 framework<sup>†</sup>

Xiufang Li,<sup>a</sup> Yanxi Tan,<sup>a,b</sup> Zhanfeng Ju, <sup>b</sup> Wenjing Wang <sup>\*a,b</sup> and Daqiang Yuan <sup>\*a,b</sup>

The efficient separation of deuterium from hydrogen remains a significant challenge due to the limitations of conventional techniques, such as cryogenic distillation and the Girdler-sulfide process combined with electrolysis, which are characterized by substantial energy demands and relatively low separation coefficients. In contrast, the quantum sieving effect, based on porous materials, offers a promising approach to overcoming these challenges. This study presents a novel application of strong adsorption sites ( $\mu_3\text{-OH}$  group) within the nanoporous metal-organic framework of **UiO-66** for hydrogen isotope separation. By incorporating diverse organic functional groups into **UiO-66**, we successfully synthesized four derivative materials: **UiO-66-NH<sub>2</sub>**, **UiO-66-CH<sub>3</sub>**, **UiO-66-NO<sub>2</sub>**, and **UiO-66-Ph**. Experimental data reveal that the introduction of these functional groups modulated the material's pore size and channel polarity, significantly impacting its adsorption and separation performance for hydrogen isotopes. Notably, **UiO-66-NH<sub>2</sub>**, with the smallest pore size and highest channel polarity, exhibited superior hydrogen isotope adsorption capacity and selectivity, highlighting its potential as an effective adsorbent for isotope separation.

Received 5th November 2024,  
Accepted 2nd December 2024

DOI: 10.1039/d4qi02802c

[rsc.li/frontiers-inorganic](http://rsc.li/frontiers-inorganic)

## Introduction

Deuterium (<sup>2</sup>H, D), a stable isotope of hydrogen (<sup>1</sup>H, H), has been widely utilized in modern industry, scientific research, and as a fuel for nuclear fusion.<sup>1–5</sup> However, its extremely low natural abundance (0.0156%) and near-identical physico-chemical properties with other hydrogen isotopes present significant challenges for enrichment. To date, only a few large-scale techniques have been employed for the industrial purification of deuterium. These include electrolysis of heavy water extracted *via* the Girdler-sulfide process and cryogenic distillation at 24 K. Both methods are known to be highly time-consuming and energy-intensive, with relatively low separation efficiencies. This necessitates the exploration of alternative approaches that can meet the requirements for sustainable deuterium production.<sup>6</sup>

One of the most promising alternatives for D<sub>2</sub>/H<sub>2</sub> separation is quantum sieving (QS) based on nanoporous materials.

Kinetic quantum sieving (KQS) and chemical affinity quantum sieving (CAQS) effects are often used to achieve high selectivity in hydrogen isotope separation.<sup>7–20</sup> KQS occurs when the difference between pore size and molecular size becomes comparable to the de Broglie wavelength under cryogenic conditions, leading to faster D<sub>2</sub> diffusion through nanoporous material channels. However, the KQS effect demonstrates significant isotope selectivity only at cryogenic temperatures, limiting its practical application. To increase operating temperature, the CAQS effect has been developed. In this process, heavier isotopes are selectively adsorbed at strong binding sites due to differences in zero-point energy (ZPE).

The most extensively studied class of CAQS materials for D<sub>2</sub>/H<sub>2</sub> separation is Metal-Organic Frameworks (MOFs).<sup>21–28</sup> MOFs allow for flexible adjustment of pore size and open metal sites to achieve high D<sub>2</sub>/H<sub>2</sub> selectivity. Some MOFs with a high density of metal open sites have successfully achieved efficient D<sub>2</sub>/H<sub>2</sub> separation. However, most MOFs containing open metal sites suffer from limited moisture stability, as water readily attacks the metal active sites, leading to material degradation.

Therefore, effectively utilizing the CAQS effect to enhance D<sub>2</sub>/H<sub>2</sub> separation performance while maintaining MOF structural stability is a critical issue that needs addressing. **UiO-66**, a well-known zirconium(IV)-containing MOF, has attracted con-

<sup>a</sup>University of the Chinese Academy of Sciences, Beijing 100049, China

<sup>b</sup>State Key Laboratory of Structural Chemistry, Fujian Institute of Research on the Structure of Matter, Chinese Academy of Sciences, Fuzhou 350002, China.

E-mail: [wjwang@fjirs.m.ac.cn](mailto:wjwang@fjirs.m.ac.cn), [ydq@fjirs.m.ac.cn](mailto:ydq@fjirs.m.ac.cn)

<sup>†</sup> Electronic supplementary information (ESI) available. See DOI: <https://doi.org/10.1039/d4qi02802c>



siderable attention due to its exceptional stability, excellent adsorption properties, cost-effective regenerability, and good functional-group tolerance during synthesis. Despite the absence of open metal sites in **UiO-66**, the  $\mu_3\text{-OH}$  group of the  $\text{Zr}_6\text{O}_4(\text{OH})_4$  inorganic cornerstones can serve as strong interaction sites, facilitating intense interactions between the material and hydrogen or deuterium.<sup>29</sup>

Current research on CAQS primarily focuses on open metal sites, while exploration of interactions between hydrogen isotope gases and non-metal active centers remains limited. This study reports the synthesis of **UiO-66** and four of its derivatives (**UiO-66-NH<sub>2</sub>**, **UiO-66-NO<sub>2</sub>**, **UiO-66-CH<sub>3</sub>**, **UiO-66-Ph**), along with a detailed analysis of their  $\text{D}_2/\text{H}_2$  separation capabilities (Scheme 1). Our findings indicate that the incorporation of functional groups into **UiO-66** leads to improved separation performance.

## Results and discussion

The synthesis of **UiO-66** and its derivatives was conducted following a modified procedure based on previously published literature.<sup>30</sup> As shown in Fig. 1a, the powder X-ray diffraction (PXRD) patterns of the synthesized materials were compared with simulated PXRD patterns, revealing good phase purity and functional-group tolerance for **UiO-66** and its derivatives. Infrared spectroscopic analysis of the derivatives confirmed the successful incorporation of the intended functional groups, as evidenced by characteristic peaks (Fig. S1†).

The porosity of **UiO-66** and its derivatives was assessed using nitrogen adsorption isotherms at 77 K. Both **UiO-66** and its derivatives displayed typical type I isotherms, indicating their microporous structures (Fig. 1b). The nitrogen adsorption capacities were measured as follows:  $328 \text{ cm}^3 \text{ g}^{-1}$  for **UiO-66**,  $291 \text{ cm}^3 \text{ g}^{-1}$  for **UiO-66-NO<sub>2</sub>**,  $295 \text{ cm}^3 \text{ g}^{-1}$  for **UiO-66-NH<sub>2</sub>**,  $262 \text{ cm}^3 \text{ g}^{-1}$  for **UiO-66-CH<sub>3</sub>**, and  $252 \text{ cm}^3 \text{ g}^{-1}$  for **UiO-66-Ph**. The corresponding specific surface areas determined by the Brunauer–Emmett–Teller (BET) method were

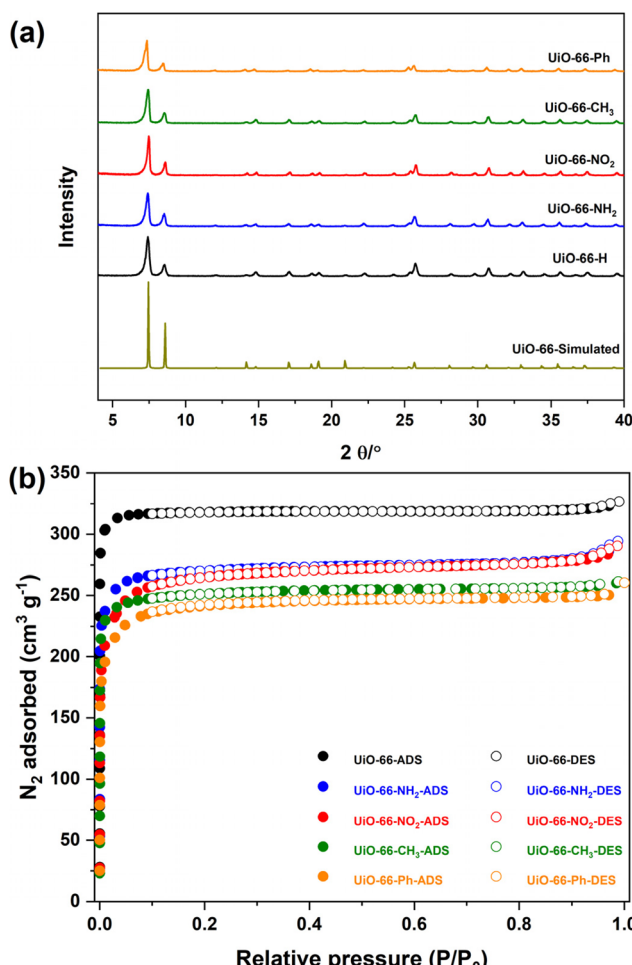
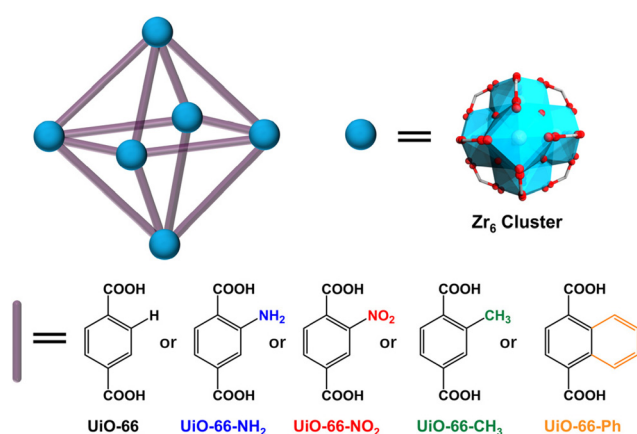


Fig. 1 (a) Simulated and observed PXRD patterns of **UiO-66** and its derivatives; (b)  $\text{N}_2$  isotherms of **UiO-66** and its derivatives at 77 K.



Scheme 1 Synthetic process of pristine **UiO-66** and its isoreticular derivatives.

found to be  $1250 \text{ m}^2 \text{ g}^{-1}$  for **UiO-66**,  $985 \text{ m}^2 \text{ g}^{-1}$  for **UiO-66-NO<sub>2</sub>**,  $1036 \text{ m}^2 \text{ g}^{-1}$  for **UiO-66-NH<sub>2</sub>**,  $960 \text{ m}^2 \text{ g}^{-1}$  for **UiO-66-CH<sub>3</sub>**, and  $902 \text{ m}^2 \text{ g}^{-1}$  for **UiO-66-Ph**. These data indicate that **UiO-66** has the highest BET surface area, with the addition of different functional groups resulting in varying degrees of reduction in specific surface area.

The pore size distribution (PSD) was further analyzed using density functional theory (DFT) calculations. The results demonstrated that the derivatives (**UiO-66-NO<sub>2</sub>**, **UiO-66-NH<sub>2</sub>**, and **UiO-66-CH<sub>3</sub>**) possess smaller pore sizes than pristine **UiO-66** (Fig. S2†). Contrary to expectations based on group size, **UiO-66-Ph** would be expected to have a smaller pore size than the other derivatives. However, the opposite result is observed. This discrepancy could be attributed to the orientation of the benzene rings and the presence of defects within the material, which together permit the formation of larger pore sizes.

The high BET values and microporous structures of **UiO-66** and its derivatives motivate our investigation into their adsorption capacities for hydrogen isotopes. The initial stage of the study involved analyzing  $\text{H}_2$  and  $\text{D}_2$  gas adsorption data at



temperatures of 77 K and 87 K (Fig. 2 and Table S1†). Due to the change in mass induced by the introduction of functional groups, the amount of adsorbed gas per unit cell was selectively used as a measure of the material's adsorption performance.

At 77 K and 110 kPa, the  $D_2$  adsorption capacities of **UiO-66-NH<sub>2</sub>** and **UiO-66-CH<sub>3</sub>** were nearly equivalent to that of **UiO-66**, with **UiO-66-NO<sub>2</sub>** showing a slight decrease and **UiO-66-Ph** exhibiting the most substantial reduction. For  $H_2$  adsorption under identical conditions, the  $H_2$  adsorption capacity of **UiO-66-NH<sub>2</sub>** was comparable to that of **UiO-66**, while both **UiO-66-CH<sub>3</sub>** and **UiO-66-NO<sub>2</sub>** experienced minor decreases, with **UiO-66-Ph** demonstrating the most significant decline. Notably, at low pressures, the  $H_2$  and  $D_2$  gas adsorption capacities of **UiO-66-NH<sub>2</sub>**, **UiO-66-NO<sub>2</sub>**, and **UiO-66-CH<sub>3</sub>** exceeded those of the pristine material **UiO-66**, indicating an enhanced interaction with hydrogen isotope gases despite the decrease in BET values.

A significant shift in isotope gas adsorption behavior was observed at 87 K. For  $D_2$  adsorption, **UiO-66-NH<sub>2</sub>** and **UiO-66-CH<sub>3</sub>** exhibited higher capacities across the entire pressure range compared to **UiO-66**. **UiO-66-NO<sub>2</sub>** showed increased adsorption in the low-pressure region, with its capacity at 110 kPa nearly matching that of **UiO-66**, while **UiO-66-Ph** maintained a lower capacity throughout. The  $H_2$  adsorption behavior at 87 K followed a similar pattern to  $D_2$ . As the temperature rose to 87 K, the decrease in  $H_2$  and  $D_2$  adsorption performance for **UiO-66-NH<sub>2</sub>** and **UiO-66-CH<sub>3</sub>** was less than that of **UiO-66**, suggesting that organic functional groups effectively enhanced the material's affinity for hydrogen isotopes. The reduced adsorption performance of **UiO-66-Ph** can be primarily attributed to its lower specific surface area and microporous volume (Table S1†).

Additionally,  $D_2$  adsorption capacities at both 77 K and 87 K were higher than those of  $H_2$ , pointing to quantum effects. The isotherms for both  $H_2$  and  $D_2$  adsorption comple-

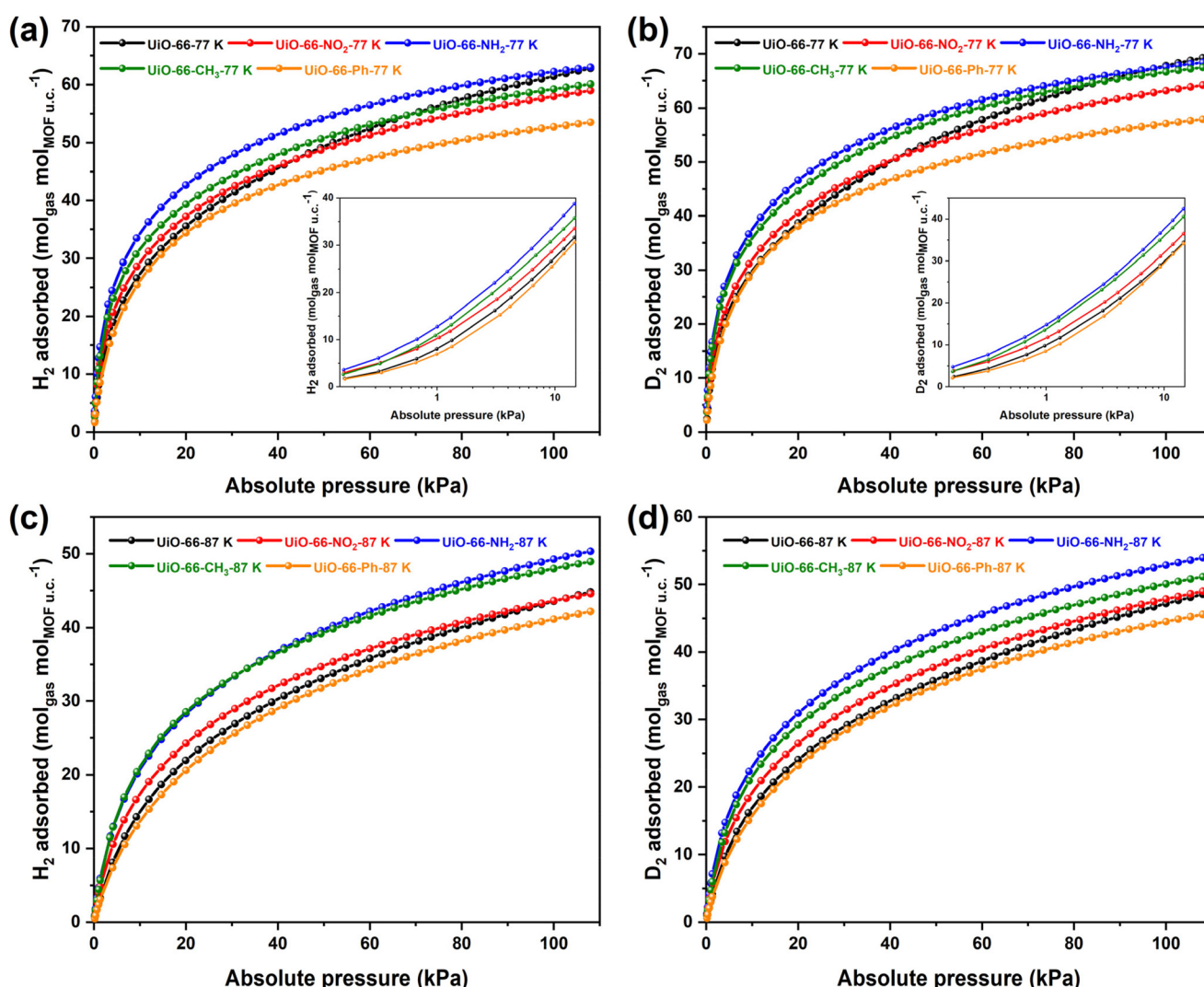


Fig. 2 (a) 77 K  $H_2$ ; (b) 77 K  $D_2$ ; (c) 87 K  $H_2$  and (d) 87 K  $D_2$  adsorption isotherms of **UiO-66** and its derivatives. Inset: Enlarged perspective on the low-pressure section of the adsorption isotherms for  $H_2$  and  $D_2$  at 77 K.



tely overlapped, indicating no diffusion barrier for hydrogen isotopes within the pores. The primary cause of the differential adsorption between  $H_2$  and  $D_2$  is attributed to strong adsorption sites, predominantly driven by the interaction between the hydrogen isotope gases and the  $\mu_3\text{-OH}$  group of the  $Zr_6O_4(\text{OH})_4$  inorganic cornerstones. The incorporation of organic functional groups ( $-\text{NH}_2$ ,  $-\text{CH}_3$ ,  $-\text{NO}_2$ ) has effectively modulated pore size and polarity, further enhancing the material's interaction with isotope gases.

To gain further insight into the affinity of **UiO-66** and its derivatives for hydrogen isotopes, the isosteric heats of adsorption ( $Q_{st}$ ) were calculated (Fig. S3–S14†). At zero loading, the  $Q_{st}$  values for  $D_2$  in **UiO-66-NH<sub>2</sub>** (9.3  $\text{kJ mol}^{-1}$ ), **UiO-66-NO<sub>2</sub>** (8.9  $\text{kJ mol}^{-1}$ ), and **UiO-66-CH<sub>3</sub>** (9.0  $\text{kJ mol}^{-1}$ ) were higher than those of pristine **UiO-66** (8.7  $\text{kJ mol}^{-1}$ ). Notably, the  $Q_{st}$  value for  $D_2$  in **UiO-66-NH<sub>2</sub>** exceeds that of some porous materials reported in the literature, such as **USTC-700** (4.0  $\text{kJ mol}^{-1}$ ),<sup>31</sup> **FJI-Y9** (6.2  $\text{kJ mol}^{-1}$ ),<sup>32</sup> **FJI-Y11** (7.9  $\text{kJ mol}^{-1}$ ),<sup>33</sup> **FIR-29** (6.1  $\text{kJ mol}^{-1}$ ),<sup>32</sup> **Co(pyz)[Pt(CN)<sub>4</sub>]** (8.0  $\text{kJ mol}^{-1}$ ),<sup>34</sup> and **Cu-BDC-NH<sub>2</sub>** (7.1  $\text{kJ mol}^{-1}$ ).<sup>35</sup> The high adsorption enthalpy of **UiO-66-NH<sub>2</sub>** is predominantly attributed to its smaller pore size distribution and channel polarity. However, the  $Q_{st}$  value for  $D_2$  in **UiO-66-Ph** (8.3  $\text{kJ mol}^{-1}$ ) was lower than that in **UiO-66** due to its low pore volume and reduced channel polarity. These findings are similarly applicable to the  $Q_{st}$  values of  $H_2$ . Compared with **UiO-66** and other derivatives, a larger  $\Delta Q_{st}$  (0.6  $\text{kJ mol}^{-1}$ ) between  $D_2$  and  $H_2$  in **UiO-66-NH<sub>2</sub>** suggests that this material may possess good  $D_2/H_2$  separation properties.

To investigate the practical separation performance of **UiO-66-NH<sub>2</sub>**, breakthrough studies were conducted on  $D_2/H_2/\text{Ne}$  (3-3-94, v/v) ternary mixtures at 77 K (Fig. S15–S18†). The results showed that  $H_2$  broke through the adsorption bed first, followed by a time lag before  $D_2$  slowly eluted and reached equilibrium. This indicates that **UiO-66-NH<sub>2</sub>** preferentially adsorbs  $D_2$  over  $H_2$ . Additionally, a roll-up behavior for  $H_2$  was observed, likely due to the partial replacement of adsorbed  $H_2$  on the adsorption sites by more strongly adsorbing  $D_2$  in the gas mixture (Fig. 3a).

Furthermore, the separation performance of **UiO-66** and other derivatives has also been characterized. Breakthrough experiments suggest that materials modified with organic functional groups generally show improved separation performance. However, while **UiO-66-CH<sub>3</sub>**, **UiO-66-NO<sub>2</sub>**, and **UiO-66-Ph** exhibited increased separation coefficients compared to **UiO-66**, they experienced a decrease in  $H_2$  adsorption capacity to varying degrees. In contrast, **UiO-66-NH<sub>2</sub>** maintained high  $D_2$  adsorption capacity while also enhancing selectivity. For an equimolar mixture of  $D_2/H_2$ , the calculated separation factor was 1.38 (Fig. 3b, Table S2†). For practical industrial application, it is crucial that the ideal adsorbent have good recycling performance. Multiple  $D_2/H_2$  mixed-gas dynamic breakthrough experiments were performed under consistent operating conditions. The separation performance of  $D_2/H_2$  did not significantly change within three continuous cycles, indicating that **UiO-66-NH<sub>2</sub>** is robust and a promising candidate for  $D_2/H_2$  separation (Fig. S19†).

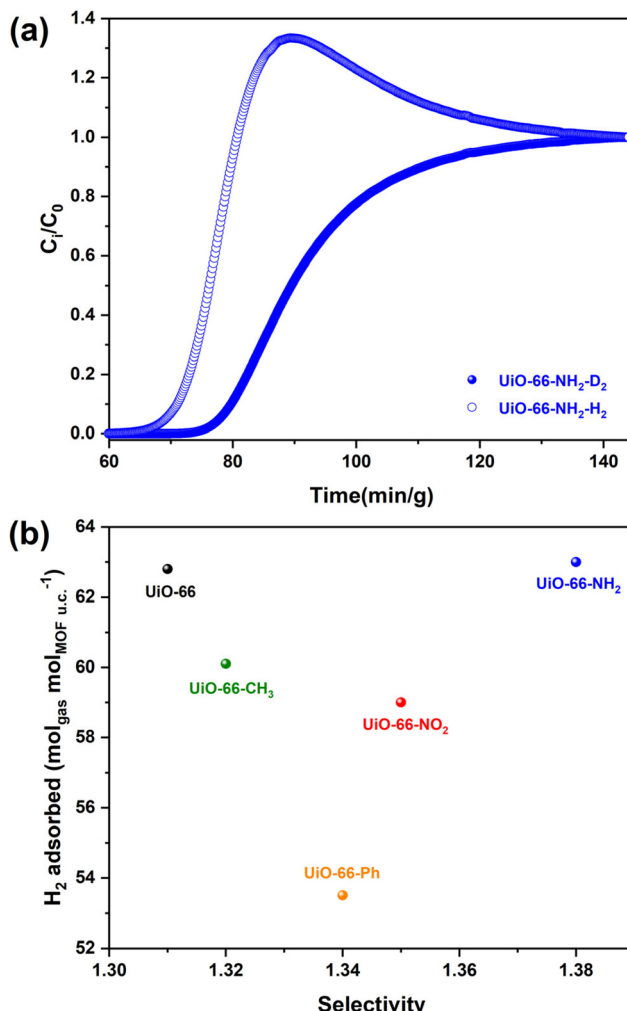


Fig. 3 (a) The dynamic breakthrough curves of **UiO-66-NH<sub>2</sub>**; (b) comparison of  $H_2$  uptake and separation factor for **UiO-66** and its derivatives.

## Conclusions

This study delves into the influence of incorporating various organic functional groups into the **UiO-66** framework on the adsorption–separation efficiency for hydrogen isotopes. The findings substantiate that by selectively modifying the pore size and channel polarity through the strategic introduction of organic functional groups, a substantial enhancement in the material's affinity for hydrogen isotopes can be achieved, thereby improving its overall separation performance. Notably, **UiO-66-NH<sub>2</sub>** emerges as an outstanding candidate due to its high capacity for adsorbing hydrogen isotopes and superior selectivity. This research underscores that, aside from the presence of metal open sites, precise adjustment of pore size and channel polarity is a viable strategy to elevate the separation performance of hydrogen isotopes in CAQS studies. **UiO-66-NH<sub>2</sub>** demonstrates exceptional potential for isotope separation applications, highlighting the importance of tailored material modifications in enhancing adsorption–separation efficiency.



## Experimental

### Materials and general methods

Infrared (IR) spectra were collected using KBr pellets over a range of 3000–400  $\text{cm}^{-1}$ , recorded on a Nicolet Magna 750 FT-IR spectrometer. Powder X-ray diffraction (PXRD) patterns were obtained using Cu K $\alpha$  radiation ( $\lambda = 1.5406 \text{ \AA}$ ) on a Rigaku Mini 600 X-ray diffractometer. Gas adsorption–desorption measurements were conducted with an automatic volumetric adsorption apparatus (Micromeritics, ASAP2020 PLUS).

### Synthesis of UiO-66 and its derivatives

In a typical synthesis, terephthalic acid (9.3 mg, 0.08 mmol) and  $\text{ZrCl}_4$  (13.2 mg, 0.04 mmol) were ultrasonically dissolved in a 10 mL solution of *N,N*-dimethylformamide (DMF), followed by the addition of 2.3 mL of acetic acid. The resulting mixture was then transferred into a sealed vial and heated at 120 °C for 24 hours. After gradually cooling to room temperature, the white powders were collected. Yield: 7.5 mg, 80%. Synthesis of other derivatives followed a similar procedure, with substitutions on the terephthalic acid to introduce the corresponding functional groups on the organic ligand.

### Breakthrough measurements

The breakthrough experiments were carried out using a dynamic gas breakthrough equipment (BSD Instrument, BSD-MAB). Activated samples were carefully transferred into a 2 mL quartz column, which was sealed at both ends with quartz wool. The column was subsequently heated to 100 °C for 12 hours, with a flow of Ne gas at 8  $\text{mL min}^{-1}$  passing through it. Prior to the measurement, the column was pre-cooled by immersed in a Dewar flask containing liquid nitrogen for approximately 20 minutes. After this preparation, a gas mixture of  $\text{H}_2/\text{D}_2/\text{Ne}$  (3/3/94, vol%) was introduced into the column at a flow rate of 15  $\text{mL min}^{-1}$ . The inlet gas flow was precisely managed by a mass flow controller (MFC), and the outlet gas composition was continuously monitored using a mass spectrometer. To regenerate the sample, it was purged with Ne gas at 10  $\text{mL min}^{-1}$  at a temperature of 100 °C for 120 minutes.

## Data availability

The data supporting this article have been included as part of the ESI.†

## Conflicts of interest

There are no conflicts to declare.

## Acknowledgements

This work was supported by National Nature Science Foundation of China (22275191, 22275186); the Self-deploy-

ment Project Research Program of Haixi Institutes, Chinese Academy of Sciences (CXZX-2022-GH01, CXZX-2022-JQ11); the Nature Science Foundation of Fujian Province (No. 2022I0037).

## References

- M. Glugla, R. Lässer, L. Dörr, D. K. Murdoch, R. Haange and H. Yoshida, The inner deuterium/tritium fuel cycle of ITER, *Fusion Eng. Des.*, 2003, **69**, 39–43.
- R. Smith, D. A. J. Whittaker, B. Butler, A. Hollingsworth, R. E. Lawless, X. Lefebvre, S. A. Medley, A. I. Parracho and B. Wakeling, Hydrogen isotope separation for fusion power applications, *J. Alloys Compd.*, 2015, **645**, S51–S55.
- I. V. Stiopkin, C. Weeraman, P. A. Pieniazek, F. Y. Shalhout, J. L. Skinner and A. V. Benderskii, Hydrogen bonding at the water surface revealed by isotopic dilution spectroscopy, *Nature*, 2011, **474**, 192–195.
- G. Zaccai, How Soft Is a Protein? A Protein Dynamics Force Constant Measured by Neutron Scattering, *Science*, 2000, **288**, 1604–1607.
- M. V. Ananyev, A. S. Farlenkov and E. K. Kurumchin, Isotopic exchange between hydrogen from the gas phase and proton-conducting oxides: Theory and experiment, *Int. J. Hydrogen Energy*, 2018, **43**, 13373–13382.
- L. Matei, C. Postolache, G. Bubueanu and C. Podina, Synthesis of Labeled Compounds Using Recovered Tritium from Expired Beta Light Sources, *Fusion Sci. Technol.*, 2017, **54**, 643–646.
- J. J. M. Beenakker, V. D. Borman and S. Y. Krylov, Molecular transport in subnanometer pores: zero-point energy, reduced dimensionality and quantum sieving, *Chem. Phys. Lett.*, 1995, **232**, 379–382.
- S. A. FitzGerald, C. J. Pierce, J. L. Rowsell, E. D. Bloch and J. A. Mason, Highly selective quantum sieving of  $\text{D}_2$  from  $\text{H}_2$  by a metal-organic framework as determined by gas manometry and infrared spectroscopy, *J. Am. Chem. Soc.*, 2013, **135**, 9458–9464.
- H. Oh and M. Hirscher, Quantum Sieving for Separation of Hydrogen Isotopes Using MOFs, *Eur. J. Inorg. Chem.*, 2016, **2016**, 4278–4289.
- I. Krkljus, T. Steriotis, G. Charalambopoulou, A. Gotzias and M. Hirscher,  $\text{H}_2/\text{D}_2$  adsorption and desorption studies on carbon molecular sieves with different pore structures, *Carbon*, 2013, **57**, 239–247.
- H. Oh, K. S. Park, S. B. Kalidindi, R. A. Fischer and M. Hirscher, Quantum cryo-sieving for hydrogen isotope separation in microporous frameworks: an experimental study on the correlation between effective quantum sieving and pore size, *J. Mater. Chem. A*, 2013, **1**, 3244–3248.
- J. Y. Kim, L. Zhang, R. Balderas-Xicohténcatl, J. Park, M. Hirscher, H. R. Moon and H. Oh, Selective Hydrogen Isotope Separation via Breathing Transition in MIL-53(Al), *J. Am. Chem. Soc.*, 2017, **139**, 17743–17746.
- D. He, L. Zhang, T. Liu, R. Clowes, M. A. Little, M. Liu, M. Hirscher and A. I. Cooper, Hydrogen Isotope Separation



Using a Metal-Organic Cage Built from Macrocycles, *Angew. Chem., Int. Ed.*, 2022, **61**, e202202450.

14 H. Oh, S. B. Kalidindi, Y. Um, S. Bureekaew, R. Schmid, R. A. Fischer and M. Hirscher, A cryogenically flexible covalent organic framework for efficient hydrogen isotope separation by quantum sieving, *Angew. Chem., Int. Ed.*, 2013, **52**, 13219–13222.

15 M. Liu, L. Zhang, M. A. Little, V. Kapil, M. Ceriotti, S. Yang, L. Ding, D. L. Holden, R. Balderas-Xicohténcatl, D. He, R. Clowes, S. Y. Chong, G. Schütz, L. Chen, M. Hirscher and A. I. Cooper, Barely porous organic cages for hydrogen isotope separation, *Science*, 2019, **366**, 613–620.

16 R. Xiong, J. Chen, L. Zhang, P. Li, X. Yan, Y. Song, W. Luo, T. Tang, G. Sang and M. Hirscher, Hydrogen isotopes separation in Ag(I) exchanged ZSM-5 zeolite through strong chemical affinity quantum sieving, *Microporous Mesoporous Mater.*, 2021, **313**, 110820.

17 J. Y. Kim, H. Oh and H. R. Moon, Hydrogen Isotope Separation in Confined Nanospaces: Carbons, Zeolites, Metal-Organic Frameworks, and Covalent Organic Frameworks, *Adv. Mater.*, 2019, **31**, e1805293.

18 L. Bondorf, J. L. Fiorio, V. Bon, L. Zhang, M. Maliuta, S. Ehrling, I. Senkovska, J. D. Evans, J.-O. Joswig, S. Kaskel, T. Heine and M. Hirscher, Isotope-selective pore opening in a flexible metal-organic framework, *Sci. Adv.*, 2022, **8**, eabn7035.

19 R. Muhammad, S. Jee, M. Jung, J. Park, S. G. Kang, K. M. Choi and H. Oh, Exploiting the Specific Isotope-Selective Adsorption of Metal-Organic Framework for Hydrogen Isotope Separation, *J. Am. Chem. Soc.*, 2021, **143**, 8232–8236.

20 J. Teufel, H. Oh, M. Hirscher, M. Wahiduzzaman, L. Zhechkov, A. Kuc, T. Heine, D. Denysenko and D. Volkmer, MFU-4 - a metal-organic framework for highly effective H<sub>2</sub>/D<sub>2</sub> separation, *Adv. Mater.*, 2013, **25**, 635–639.

21 J. Y. Kim, R. Balderas-Xicohtencatl, L. Zhang, S. G. Kang, M. Hirscher, H. Oh and H. R. Moon, Exploiting Diffusion Barrier and Chemical Affinity of Metal-Organic Frameworks for Efficient Hydrogen Isotope Separation, *J. Am. Chem. Soc.*, 2017, **139**, 15135–15141.

22 M. Jung, J. Park, R. Muhammad, J. Y. Kim, V. Grzimek, M. Russina, H. R. Moon, J. T. Park and H. Oh, Elucidation of Diffusivity of Hydrogen Isotopes in Flexible MOFs by Quasi-Elastic Neutron Scattering, *Adv. Mater.*, 2021, **33**, e2007412.

23 L. Zhang, S. Jee, J. Park, M. Jung, D. Wallacher, A. Franz, W. Lee, M. Yoon, K. Choi, M. Hirscher and H. Oh, Exploiting Dynamic Opening of Apertures in a Partially Fluorinated MOF for Enhancing H<sub>2</sub> Desorption Temperature and Isotope Separation, *J. Am. Chem. Soc.*, 2019, **141**, 19850–19858.

24 I. Savchenko, A. Mavrandonakis, T. Heine, H. Oh, J. Teufel and M. Hirscher, Hydrogen isotope separation in metal-organic frameworks: Kinetic or chemical affinity quantum-sieving?, *Microporous Mesoporous Mater.*, 2015, **216**, 133–137.

25 H. Oh, I. Savchenko, A. Mavrandonakis, T. Heine and M. Hirscher, Highly Effective Hydrogen Isotope Separation in Nanoporous Metal-Organic Frameworks with Open Metal Sites: Direct Measurement and Theoretical Analysis, *ACS Nano*, 2014, **8**, 761–770.

26 X. Li, X. Wang, M. Li, J. Luo, Y. An, P. Li, J. Song, C. Chen, X. Feng and S. Wang, Highly selective adsorption of D<sub>2</sub> from hydrogen isotopes mixture in a robust metal bistrizolate framework with open metal sites, *Int. J. Hydrogen Energy*, 2020, **45**, 21547–21554.

27 I. Weinrauch, I. Savchenko, D. Denysenko, S. M. Souliou, H. H. Kim, M. Le Tacon, L. L. Daemen, Y. Cheng, A. Mavrandonakis, A. J. Ramirez-Cuesta, D. Volkmer, G. Schütz, M. Hirscher and T. Heine, Capture of heavy hydrogen isotopes in a metal-organic framework with active Cu(I) sites, *Nat. Commun.*, 2017, **8**, 14496.

28 I. Krkljus and M. Hirscher, Characterization of hydrogen/deuterium adsorption sites in nanoporous Cu-BTC by low-temperature thermal-desorption mass spectroscopy, *Microporous Mesoporous Mater.*, 2011, **142**, 725–729.

29 S. Chavan, J. G. Vitillo, D. Gianolio, O. Zavorotynska, B. Civalleri, S. Jakobsen, M. H. Nilsen, L. Valenzano, C. Lamberti, K. P. Lillerud and S. Bordiga, H<sub>2</sub> storage in isostructural UiO-67 and UiO-66 MOFs, *Phys. Chem. Chem. Phys.*, 2012, **14**, 1614–1626.

30 Y. Huang, W. Qin, Z. Li and Y. Li, Enhanced stability and CO<sub>2</sub> affinity of a UiO-66 type metal-organic framework decorated with dimethyl groups, *Dalton Trans.*, 2012, **41**, 9283–9285.

31 Q. Yan, J. Wang, L. Zhang, J. Liu, M. Wahiduzzaman, N. Yan, L. Yu, R. Dupuis, H. Wang, G. Maurin, M. Hirscher, P. Guo, S. Wang and J. Du, A squareate-pillared titanium oxide quantum sieve towards practical hydrogen isotope separation, *Nat. Commun.*, 2023, **14**, 4189.

32 F. J. Zhao, Y. X. Tan, W. Wang, Z. Ju and D. Yuan, Optimizing H<sub>2</sub>, D<sub>2</sub>, and C<sub>2</sub>H<sub>2</sub> Sorption Properties by Tuning the Pore Apertures in Metal-Organic Frameworks, *Inorg. Chem.*, 2018, **57**, 13312–13317.

33 Y. Si, X. He, J. Jiang, Z. Duan, W. Wang and D. Yuan, Highly effective H<sub>2</sub>/D<sub>2</sub> separation in a stable Cu-based metal-organic framework, *Nano Res.*, 2019, **14**, 518–525.

34 J. Ha, M. Jung, J. Park, H. Oh and H. R. Moon, Thermodynamic Separation of Hydrogen Isotopes Using Hofmann-Type Metal-Organic Frameworks with High-Density Open Metal Sites, *ACS Appl. Mater. Interfaces*, 2022, **14**, 30946–30951.

35 A. Dastbaz, J. Karimi-Sabet, Y. Amini and M. A. Moosavian, A comprehensive study on the kinetics and isotherms of D<sub>2</sub>/H<sub>2</sub> adsorptive separation using pure and composite Cu-BDC-NH<sub>2</sub> MOFs at 77 K, *Int. J. Hydrogen Energy*, 2024, **61**, 893–900.